Combustion and Flame 157 (2010) 2298–2305

Contents lists available at ScienceDirect

Combustion and Flame

journal homepage: www.elsevier.com/locate/combustflame

Plasma assisted flame ignition of supersonic flows over a flat wall

Hyungrok Do *, Seong-kyun Im, Mark A. Cappelli, M. Godfrey Mungal

Mechanical Engineering Department, Stanford University, Stanford, California 94305-3032, United States

ARTICLE INFO

Article history:
Received 14 April 2010
Received in revised form 26 May 2010
Accepted 7 July 2010

Keywords:
Scramjet
Plasma assisted combustion
Supersonic
Pulsed plasma
Ethylene
Flat wall

ABSTRACT

A nanosecond pulsed plasma discharge located between two fuel jets is used to ignite and hold jet flames in supersonic crossflows, without the use of additional devices (e.g., cavities or backsteps) for flame holding. The fuel injection nozzles and discharge electrodes are mounted flush with the surface of the flat wall adjacent to the freestream flow. The nonequilibrium plasma is produced by repetitive pulses of 15 kV peak voltage, 10 ns pulse width and 50 kHz repetition rate. Sonic or subsonic fuel jets (hydrogen and ethylene) are injected into a pure oxygen freestream of Mach numbers Ma = 1.7–2.4. The shockwave/flow structures induced by the fuel jets and the OH radical distribution resulting from combustion are characterized by Schlieren photography and planar laser induced fluorescence imaging, respectively. A configuration combining an upstream subsonic oblique jet and a downstream sonic transverse jet is shown to provide adequate flow conditions for jet flame ignition assisted by the plasma discharge. The experimental results are interpreted using a simple model by which the pulsed plasma serves as a source of reactive radicals added to a flammable gas mixture.

1. Introduction

Flame stabilization in supersonic flows is of critical importance to the development of scramjet engines for use on hypersonic aircraft. Typical approaches for sustaining combustion in such high speed flows are methods that provide recirculation zones that produce low speed regions where a flame is able to reside. These recirculating flow regions act by increasing the flow residence time (τ_{res}) in a combustor and enhancing fuel/oxidizer mixing. The flow residence time should be longer than the ignition delay time (τ_{ign}) to initiate/sustain combustion reactions. Typical flame stabilization methods often include geometric surface alterations to generate recirculation regions, such as the addition of cavities [1–3], ramp injectors [4,5], wall steps [6] and angled combustor walls [7]. However, in supersonic flow environments, the stagnation pressure loss sustained by the use of such wall features can result in a significant loss of thrust.

There has been a growing interest in using nonequilibrium plasma discharges for flame stabilization in subsonic [8–17] and supersonic [6,7,18] environments. These discharges have a high propensity to produce reactive radical species. The radical species in flammable mixtures facilitate combustion reactions to reduce the ignition delay time [19]. While nonequilibrium plasmas alone can be beneficial to flame stabilization, however, they are most often used in conjunction with wall features in supersonic flows to guarantee stable combustion. For example, in the studies of Rogers et al. [7], an arc jet was injected into the downstream region of a fuel injection ramp, and in the work of Leonov et al. [6], a quasi direct-current (DC) discharge plasma was generated within a surface cavity, in both cases, to stabilize combustion.

Our study is focused on developing a method that employs nonequilibrium pulsed plasmas for supersonic combustion stabilization without the simultaneous use of geometric wall features. Here, we describe a dual fuel jet injection configuration where the plasma discharge is located on a flat wall between an upstream oblique subsonic fuel jet and a downstream transverse sonic fuel jet. The upstream jet seeds the hot boundary layer with fuel, producing a stream that is ignited by the plasma discharge and that then serves as a pilot flame radical source to initiate combustion reaction in the main downstream jet. Consequently, a localized plasma discharge (10 W average power in approximately 6 mm^3 discharge volume) is capable of igniting a flame of almost 10^5 times greater combustion energy release [20].

2. Experimental setup

An expansion tube is used to simulate the high enthalpy supersonic flow in the combustor of a scramjet engine. Details of the expansion tube are provided in Ref. [21] and only a brief description is given here. The expansion tube is a circular stainless steel tube of 14 cm inner diameter connected to a cylindrical dump tank (60 cm diameter and 122 cm length). The tube has three sections separated by two breakable diaphragms. These include the driver

* Corresponding author. Address: Bldg. 520, Room 520I, Stanford, CA 94305-3032, United States. Fax: +1 650 723 1748.
E-mail address: hyungrok@stanford.edu (H. Do).

0010-2180/$ - see front matter © 2010 The Combustion Institute. Published by Elsevier Inc. All rights reserved.
doi:10.1016/j.combustflame.2010.07.006

section (2 m in length), the driven section (7.3 m in length), and the expansion section (2.8 m in length). Prior to operation, the driven section is filled with the desired test gas, i.e., the gas that will flow across the model in the test section during the run time. The driver and expansion sections are filled with high and low pressure helium, respectively. When the primary diaphragm separating the driver and driven sections ruptures, a shockwave propagates through the driven section elevating the temperature and pressure of the test gas. The elevated pressure in the driven section subsequently ruptures the second diaphragm, releasing the test gas to undergo an unsteady expansion and flow through the lower pressure test section which houses a test model (see below). A test section (welded stainless steel cube, 30 cm × 30 cm × 30 cm inside dimensions), for observations and measurements is located between the expansion section and the dump tank. Each flow condition corresponds to a specific combination of initial pressures in the three tube sections, as indicated in Table 1. Additional parameters can be found in Ref. [22].

A flat wall jet in crossflow model is installed in the test section. The schematic of the flat wall model is shown in Fig. 1. The model, simulating the wall of a supersonic combustor in a scramjet engine, is a rectangular aluminum plate (14 × 10 cm, 2.5 cm thickness) containing two jet injection nozzles (2 mm diameter), electrodes and an embedded ceramic plate for electrical insulation of the pulsed discharge electrodes. A heat-treated 22° angle sharp leading edge (A2 tool steel) is attached on the front side of the model flush with the upper surface. The model is a cavity-free flat surface. The injection nozzles are drilled holes in the aluminum plate separated by 26 mm in the streamwise direction. A ceramic plate (1.5 cm × 2.5 cm) containing the two holes for accommodating the electrodes (1 mm diameter, 2% thoriated tungsten rods) separated in the streamwise direction by 6 mm is embedded between the two jet nozzles. The ceramic plate and the electrodes are flush with the surface of the model. The two nozzles and the two electrodes are aligned along the center line of top surface of the model. The upstream jet injection nozzle is positioned 1 cm upstream of the nearest electrode.

A nonequilibrium plasma is produced by high voltage pulses (typically 15 kV peak voltage, 10 ns pulse width and 50 kHz repetition rate, i.e., 20 μs pulse period) applied between the two electrodes. The cathode is negatively biased (−7.5 kV) while the anode is positively biased (+7.5 kV) at the peaks of the pulses. The voltage pulses are formed by a pulse generator (FID Technology, Model F1112) powered by two DC power supplies and triggered by a high speed switching circuit. A high voltage DC power supply (Sorensen, Model DCS600-1.7E) provides the main power consumed by the plasma and the plasma generation system. A supplemental DC power supply (HP, Model 6264B) is used for providing power to a refrigeration system for cooling the pulse generator.

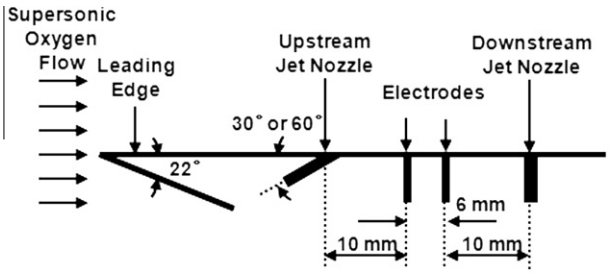

Fig. 1. A schematic of a jet in crossflow model.

OH planar laser induced fluorescence (PLIF) is used to visualize the ground state OH radical distribution following flame ignition. The characterization of the ground state OH distribution provides a qualitative indicator of the presence of combustion and the physical location of the flame region. A Nd:YAG laser (Continuum Precision, Model PL8000) that pumps a dye laser (Lumonics, Model HD-500) equipped with a frequency doubling unit (Lumonics, Model HyperTRAK-1000) for generating 3–7 mJ per pulse at 283 nm (10 Hz repetition rate), is used to excite the A-X(1,0) Q1(7) electronic transition of the OH molecule. The laser beam is transformed into a thin sheet by a set of cylindrical concave and spherical convex lenses. The sheet of the laser beam is projected vertically, through a quartz window on the upper face of the test section, on the center line of the model's surface, in a plane coincident with the electrodes and jet injection nozzle. The spectrally filtered (using a narrow band pass filter from 305 to 325 nm) laser induced fluorescence is captured by an intensified camera (Andor, iStar ICCD) at right angles to the plane of the laser sheet. The limiting resolution of these images is approximately 80 μm, estimated from the camera array size of 512 × 512 pixels imaged onto a 40 × 40 mm region of the flow. The images depict noncalibrated OH ground state concentration fields, which serve to provide a qualitative depiction of the flame structure. Schlieren imaging [23] is carried out with an ultra fast framing camera (Imacon 486 intensified CCD camera) and a pulsed xenon flash lamp (Hamamatsu, Model E6611).

Table 1
Pressures of the three sections corresponding to flow conditions.

Run condition		1	2	3	4
Initial pressures	Driver section (psia)	45	67	177	195
	Buffer section (psig)	–	–	75	75
	Driven section (torr)	23	10	17	19
	Expansion section (torr)	56	28	29	7
Freestream conditions	Mach number	1.7 ± 0.03	2.0 ± 0.03	2.4 ± 0.05	2.4 ± 0.05
	Stagnation enthalpy (MJ/kg)	1.0 ± 0.05	2.0 ± 0.05	2.4 ± 0.08	2.4 ± 0.08
	Static temperature (K)	900 ± 30	1250 ± 50	1240 ± 50	1300 ± 50
	Static pressure (kPa)	25 ± 1	16 ± 1	18 ± 1	24 ± 1
	Test time (μs)	700 ± 50	500 ± 50	350 ± 50	350 ± 50
	Flow velocity (m/s)	1000 ± 20	1380 ± 25	1650 ± 30	1690 ± 30
Re_D of hydrogen jet: jet to freestream momentum ratio (J) = 4 jet nozzle diameter (D) = 2 mm ($\times 10^5$)		1.39	1.23	1.99	2.65
Hydrogen Jet J_n (oxygen freestream flow)	Upstream oblique jet	–	3.5 (θ = 30°)	0.1 (θ = 60°)	0.1 (θ = 60°)
	Downstream transverse jet	–	9.5	3	2
Ethylene Jet J_n (air freestream flow)	Upstream oblique jet	–	–	0.1 (θ = 30°)	–
	Downstream transverse jet	–	–	2	–

3. Results and discussion

3.1. Flat wall flame stabilization: dual fuel jet injection

The smooth wall surface of a supersonic combustor is preferred for minimizing the stagnation pressure loss of a supersonic flow that travels through the combustor. However, it is quite challenging to hold a flame in a supersonic flow without a region of reduced velocity or recirculation provided by geometric surface features such as a cavity or a backstep. In our previous work [19], the effects of a local cavity on flame holding in a supersonic environment are studied in detail. It is found that the flame generated in the slow flow recirculation region in the cavity serves as a radical source shortening the ignition delay time of the supersonic flow outside of the cavity. Thus, to hold a flame on a flat wall, an effective radical source is needed, that is capable of surviving the supersonic freestream flow conditions. The nonequilibrium pulsed plasma discharge can serve as this radical source. Figure 2 shows a photograph of the plasma discharge (plasma emission) surviving Ma ~ 1.7 air flow (run condition 1 in Table 1: $h_0 \sim 1$ MJ/kg) on a flat wall taken from a top view. The spectrally-integrated emission of at least two plasma pulses (50 kHz frequency) is accumulated during 40 μs exposure time of an intensified fast framing camera to acquire this image. The direction of the supersonic flow is from left to the right (as for all of the images presented in this paper), and when viewed from the side, the plasma appears to be concentrated in the boundary layer region of the flow.

Flame ignition and stability enhancement is obtained by seeding this boundary layer that is excited by the discharge with fuel. The slow-moving partially-premixed flammable mixture is ignited by the discharge, and is expected to serve as a pilot for the combustion of additional fuel added downstream of the discharge. To accomplish this seeding, a subsonic and oblique fuel jet is positioned just upstream of the discharge. A transverse (sonic) fuel jet is added downstream of the discharge plasma. This downstream jet carries of the majority of the total fuel (~95%) added to the oxygen stream and its higher transverse momentum serves to penetrate the boundary layer and assist in flame propagation into the supersonic freestream flow. It also produces a local recirculation region in its windward side, facilitating the combustion of the seeded slow-moving boundary layer, and strong recirculation and re-entrainment counter-rotating vortices on the leeward side, allowing species produced by the plasma and the pilot flame to reside in the region long enough to ignite the downstream jet flame.

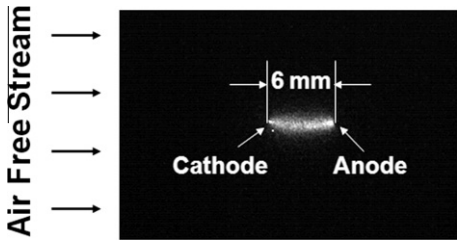

Fig. 2. Plasma emission images taken by an intensified fast framing camera with a supersonic air flow (run condition 1).

Figure 3 compares a hydrogen jet flame (run condition 2: $h_0 \sim 2.0$ MJ/kg, pure oxygen crossflow) without (Fig. 3a) and with (Fig. 3b) an oblique (30°) upstream hydrogen jet injected into the boundary layer without any plasma activation. In this study, we have focused mostly on the simplest H_2/O_2 combustion system by utilizing pure oxygen supersonic crossflows, which facilitates an analysis of the kinetics, presented in the latter part of the paper. The Schlieren photographs reveal the general features in the flow fields, and sections of these images are superimposed onto the OH PLIF images (Fig. 3c and d) to depict regions of combustion. The jet momentum ratio (J_n) is defined by:

$$J_n = \sin(\theta) \cdot \frac{(\rho u^2)_{\text{jet}}}{(\rho u^2)_{\infty}} = \sin(\theta) \cdot \frac{(\gamma p M^2)_{\text{jet}}}{(\gamma p M^2)_{\infty}}$$

Here, J_n is the ratio of the normal component of the jet momentum flux to the freestream momentum flux, respectively, θ, ρ, u, γ, p, and M are jet injection angle, density, velocity, ratio of specific heats, pressure and Mach number of the jet (subscript jet) and freestream (subscript ∞) flow. The J_n of the oblique ($\theta = 30°$) upstream jet and the transverse ($\theta = 90°$) downstream jet are approximately 3.5 and 9.5, respectively.

As seen in Fig. 3b, the intersection of the jet trajectories is located in the region adjacent to the recirculation zone in the windward side of the downstream jet. The relatively strong flame observed at this windward side recirculation zone seen in Fig. 3d enhances the combustion of the downstream jet fuel and is clearly stronger when compared to the weak fragmented flame in Fig. 3c, i.e., when there is no upstream jet. A comparison of the two OH

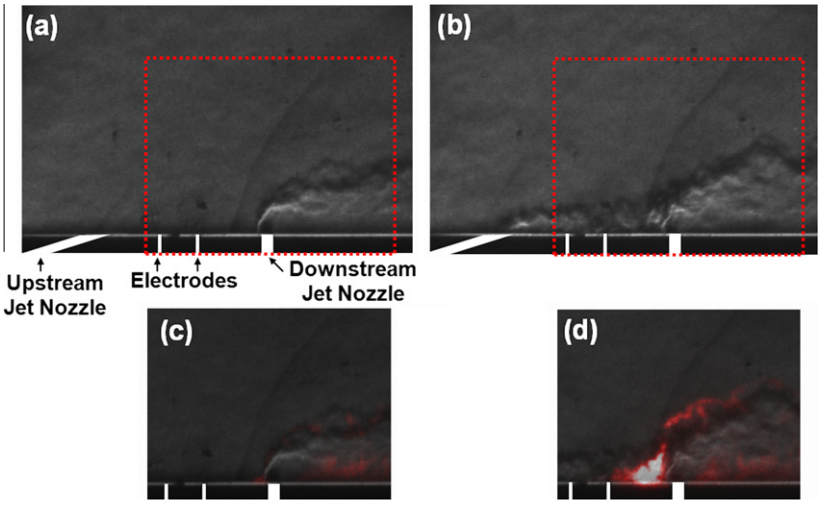

Fig. 3. Two Schlieren images illustrate flow fields (oxygen freestream flow: run condition 2) (a) without and (b) with the upstream jet ($J_n \sim 3.5$, 30° angle) in front of a downstream jet of $J_n \sim 9.5$ (90° angle). Rectangular regions indicated by red dotted lines in the Schlieren images are overlapped on OH PLIF images (c) without and (d) with the upstream jet. (For interpretation of the references to color in this figure legend, the reader is referred to the web version of this article.)

PLIF images attributes this difference to the much stronger reaction/flame observed in the windward side (with the upstream jet ignition), than that in the absence of the upstream hydrogen jet. The upstream fuel jet is injected into an oxygen boundary layer of high static temperature. This boundary layer flow is compressed by the bow shock generated by the downstream jet and produces a separated flow recirculation that promotes local flame ignition.

Downstream jet flame enhancement without a discharge plasma is not obtained when a subsonic upstream jet is injected at a (higher) 60° angle, as seen in Fig. 4, which depicts OH PLIF images superimposed onto Schlieren photographs with a pure oxygen crossflow (run condition 4: $h_0 \sim 2.4$ MJ/kg). The left panel (Fig. 4a) depicts a condition without the upstream jet and without the discharge, and the center panel (Fig. 4b) with both the subsonic upstream ($J_n = 0.1$) and sonic downstream ($J_n = 2$) jet active but still without the discharge. In the absence of both the upstream jet and discharge, there is a moderate OH signal on the windward side of the main sonic jet in the recirculation region near the surface (Fig. 4a), induced as a result of the strong bow shock. However, a rather weaker fragmented flame detached from the surface is observed with both the jets activated (Fig. 4b), while the jet flame is significantly enhanced by the plasma discharge as shown in Fig. 4c [20]. Here the cathode is placed in the upstream configuration.

The effect of the pulsed plasma on the upstream jet flame (pilot flame) is illustrated by the OH PLIF images of the near-electrode regions, presented in Fig. 5. For these images, the upstream jet injection angle is 60° from the horizontal plane, $J_n = 0.1$, and the cross stream is pure oxygen (run condition 3: $h_0 = 2.4$ MJ/kg). The left panel (Fig. 5a), taken without the discharge, reveals OH to be generated in the hot boundary layer along the electrodes and just upstream of the $J_n = 3$ transverse sonic jet. Figure 5b is similar to that of Fig. 5a, but taken 1 μs after a discharge pulse preceded by repetitive pulses (50 kHz). We see that the OH signal is enhanced by the discharge (Fig. 5b), but is not yet sufficiently robust to ignite the boundary layer mixture. With the electrodes reversed (Fig. 5c) so that the cathode precedes the anode in the streamwise direction, a strong (pilot) flame is observed by comparison, which ultimately serves to enhance the ignition and combustion of the main sonic fuel jet.

3.2. Sustaining the jet flames

A series of OH PLIF images taken at various points within the test time of the run is presented in Fig. 6. In this case, both of the upstream (60° angle, $J_n = 0.1$) and downstream jets ($J_n = 3$) are active and the crossflow is again high enthalpy oxygen (run condition 3: $h_0 = 2.4$ MJ/kg). Figure 6a–c are taken 1 μs after the first (at $t = 0$ μs: the beginning of the test time), the sixth (at 100 μs from

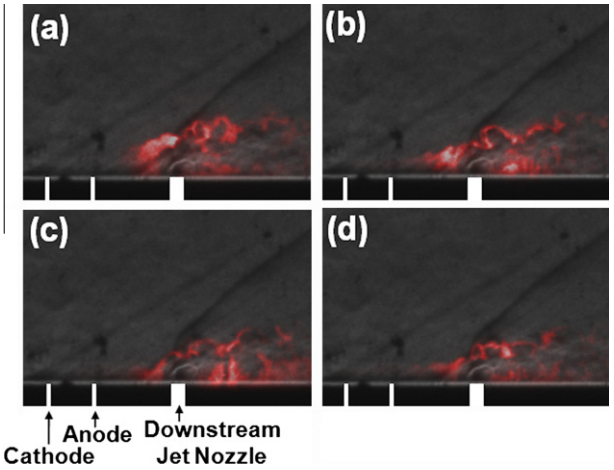

Fig. 6. OH PLIF images, overlapped on a typical Schlieren image, are taken with a pure oxygen crossflow (run condition 3): (a), (b) and (c) are taken 1 μs after a plasma pulse: (a) at the beginning of the test time, 0 μs, (b) 100 μs and (c) 200 μs after the beginning of the test time, (d) is taken 18 μs after the plasma pulse and 200 μs after the beginning of the test time. The upstream and downstream hydrogen jets are activated with corresponding jet momentum ratios of $J_n \sim 0.1$ (60° angle) and $J_n \sim 3$ (90° angle), respectively.

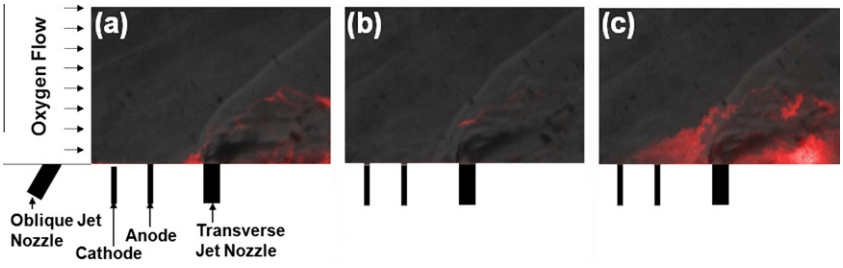

Fig. 4. The OH PLIF images overlapped with a typical Schlieren image of the same flow condition (run condition 4): (a) without the upstream jet, (b) with both jets active (upstream jet of $J_n \sim 0.1$ (60° angle) and downstream jet of $J_n \sim 2$ (90° angle)) without plasma and (c) in the presence of the plasma with both jets.

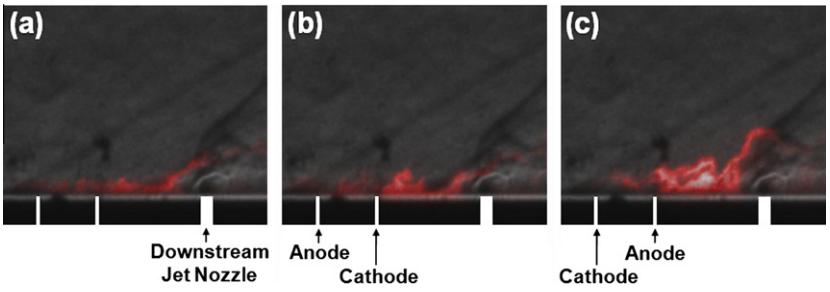

Fig. 5. The OH PLIF images, overlapped on a typical Schlieren image (run condition 3), show a small region near the electrodes and downstream jet of $J_n \sim 3$ (90° angle) with the upstream jet activated ($J_n \sim 0.1$, 60° angle): (a) without the plasma, and (b) 1 μs after a discharge pulse with anode upstream and (c) cathode upstream.

the beginning), and the eleventh (at 200 μs) plasma pulse, respectively. Plasma-enhanced pilot flames and stronger downstream jet flames in the leeward side as well as in the windward side of the downstream jet are observed. It is apparent that the plasma assisted flame is sustained during the whole test time (350 μs). Also, it is noteworthy that the plasma enhanced flame appears immediately at the start of the test time (at 0 μs, i.e., see Fig. 6a) following a discharge pulse whereas an ignition delay of about 40 μs is seen in the same facility, when a cavity was used as a flame holder, even at higher enthalpy freestream flow conditions [19]. We attribute this faster dissemination of the discharge effect to the discharge placement in high speed flows directly on the flat wall.

The OH PLIF image shown in Fig. 6d is taken 18 μs after the eleventh discharge pulse (200 μs into the test time) to demonstrate that the flame remains lit between the plasma pulses. In this image, we see that the plasma assisted flame in the windward side of the downstream jet exists, which implies that a 20 μs pulse period (50 kHz plasma repetition rate) is short enough to sustain the plasma assisted flame between the pulses.

3.3. Ethylene jet flame ignition

Figure 7 presents OH PLIF images taken (a) without and (b) in the presence of the pulsed plasma with ethylene fuel jet injection. The upstream (30° angle from the horizontal plane, $J_n = 0.1$) and downstream ($J_n = 2$) ethylene jets are injected into pure oxygen crossflow of run condition 3. The maximum downstream jet momentum ratio (J_n) achievable with the present fuel injector when operating with ethylene is approximately $J_n = 2$ because the greater pressure drop along the fuel line when compared to hydrogen. In the absence of a plasma discharge, no detectable OH was observed, even with higher enthalpy flows ($h_0 > 3.5$ MJ/kg), consistent with that reported previously [24]. As shown in the lower enthalpy case (2.4 MJ/kg) of Fig. 7a, it is not possible to ignite a flame without the discharge, whereas a downstream jet flame is readily ignited in the presence of the pulsed discharge (Fig. 7b).

3.4. Plasma modeling and reaction kinetics simulation

To assist in interpreting our experimental findings, we have carried out numerical modeling of the pulsed discharge and reaction kinetics of plasma assisted combustion in this dual hydrogen fuel jet configuration. The intent of this simulation is to provide insight into the mechanism by which such a low power plasma can ignite and sustain the jet flames in these supersonic streams.

The modeling of the highly nonequilibrium pulsed discharge requires the solution of the Boltzmann equation for the electron energy distribution function (EEDF). This is facilitated by the use of the commercially-available Boltzmann solver (BOLSIG [25]) requiring as input conditions the applied electric field, number density, and species mole fraction. The resulting EEDF provides a means of evaluating the inelastic rate coefficients for electron impact dissociation reactions using available cross sections. The BOLSIG-based calculation carried out here uses a simplified cross section set [26,27], and accounts only for the presence of the parent molecules (H_2 and O_2) in the mixture, and does not account for electron collisions with subsequent excited states and dissociation products. The rate coefficients, in accordance with the simplified initial yield calculation method proposed by Penetrante et al. [28], allow us to determine the concentrations of the species dissociated by the pulsed plasma through the following reactions (only direct H_2 and O_2 dissociation reactions by electron impact of H_2 and O_2 are considered in the current study):

$$H_2 + e \rightarrow 2H + e \quad (R1)$$

$$O_2 + e \rightarrow 2O + e \quad (R2)$$

The parameters determining the characteristics of the plasma are based on experimental discharge conditions. The peak voltage/current of the plasma pulse are measured, as shown in Fig. 8, which are 15 kV and 14 A, respectively; only the peak voltage is used to estimate the EEDF and E/N. These traces are not recorded in the presence of the supersonic flow due to the difficulties arising from the short test time. A detailed pulsed plasma characterization was conducted using the same plasma generation system by Bak et al. [29]. The reduced electric field (E/N, where, E is the electric field applied between the electrode pair and N is the number density of the neutral molecules in the plasma region) of the pulsed plasma is estimated to be approximately 300 Td. The nominal average power consumed in the plasma region between the electrodes is approximately 10 W, as estimated from the typical experimental discharge voltage and current traces. The simulation of the reaction kinetics is carried out using a MATLAB code and implemented with the Cantera toolbox (http://www.cantera.org; http://azure.caltech.edu/~dgg/cantera/ref/index.html).

3.5. Modeling of dual fuel jet injection

Figure 9 summarizes the simulation procedure and the assumptions made to analyze the complex reacting flow phenomena as a zero dimensional reaction process describing the reactions occurring in a volume (6 mm^3) moving parallel to the surface. Molecular diffusion, mixing, expansion waves behind the shocks and heat transfer are not considered, and instant (perfect) mixing is assumed within the thermally insulated volume, nominal fuel concentrations, and shock angles are prescribed, in some cases, as guided by experiments.

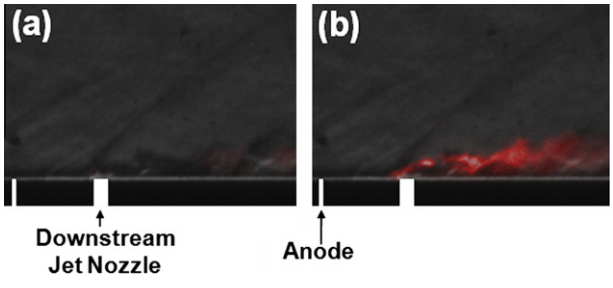

Fig. 7. OH PLIF images taken (a) without and (b) in the presence of the pulsed plasma. Both of the upstream ($J_n \sim 0.1$, 30° angle) and downstream ($J_n \sim 2$, 90° angle) ethylene jets are injected into an oxygen crossflow (run condition 3).

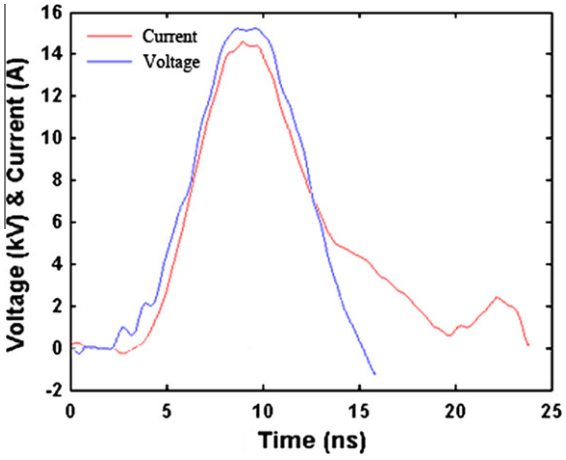

Fig. 8. Voltage and current traces recorded without supersonic flows.

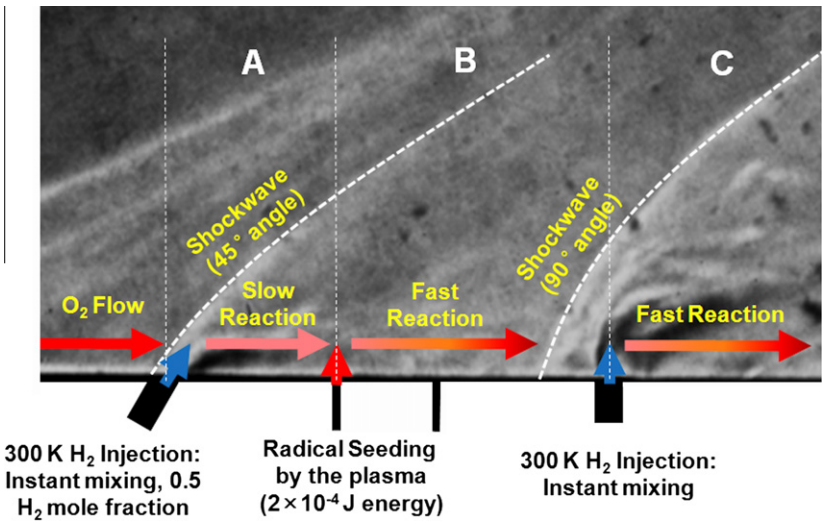

Fig. 9. Simulation procedure and assumptions for validation of the flat wall model with the dual fuel jet injection configuration.

The flow field of interest to this modeling study is divided into three parts (see Fig. 9) by (i) the upstream jet injection, (ii) seeding of the flow with the dissociated species from the pulsed plasma, and (iii) downstream jet injection. We treat the case of a pure oxygen supersonic freestream (Ma = 2.4, T_{static} = 1200 K, P_{static} = 25 kPa and h_0 = 2.5 MJ/kg). In the region between the upstream jet and the plasma discharge (region A), the freestream flow of an elevated temperature and pressure induced by the upstream jet bow shock (assumed nominally at a 45° angle) is instantly mixed with the upstream fuel jet (300 K hydrogen). The mixture then undergoes slow initiation reactions while flowing through the cathode region at 80% of the freestream flow speed. A value of 80% of the freestream velocity is selected consistent with LES simulations [30] that predict a velocity of at most 80% of that of the freestream flow in the region extending over distances of 2*D* (*D* is the jet diameter, 2 mm in this study) above a flat surface at a position 4*D* (8 mm) downstream of the jet nozzle. In region B, between the cathode and the downstream jet, the O and H radicals produced by the pulsed plasma (10 W, 50 kHz and 6 mm^3 volume) are seeded and instantly mixed with the fluid in the discharge volume (2×10^{-4} J energy deposition via the supply of the dissociated radicals). Due to the radical seeding, fast reactions occur, and in some cases, the pilot flame is ignited in this region. In region C, where the downstream jet is injected, the radical-containing mixture encounters the downstream jet-induced bow shock (nominally 90° angle assumed) and is followed by instant mixing with the 300 K hydrogen main fuel jet. In this region, we assume a mixing of 50%, i.e., the injected hydrogen is assumed to mix with 50% (by mole

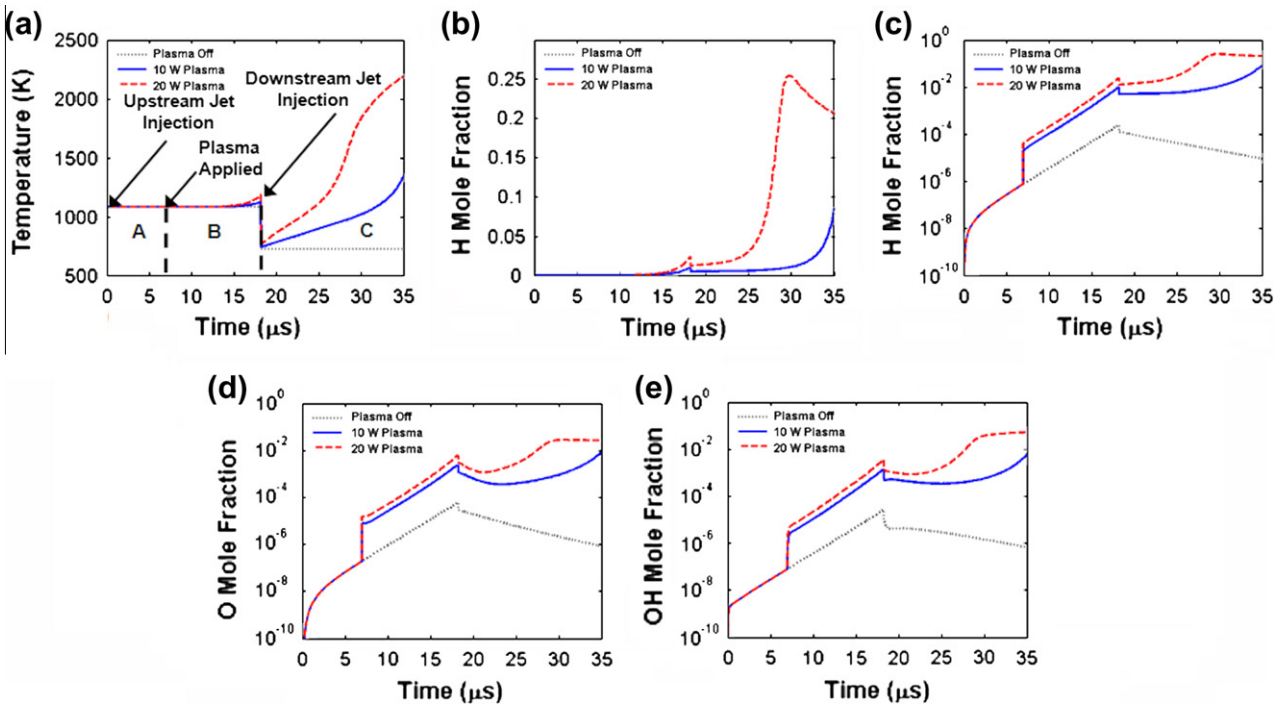

Fig. 10. Graphs of (a) temperature and radical ((b) and (c) H, (d) O, and (e) OH) mole fractions as a function of time revealing the effect of the dissociated radicals produced by the pulsed plasma.

fraction) of the incoming gas mixture from region B. The assumption of 50% mixing is ad hoc, and is not intended to represent actual mixing/diffusion characteristics. However, the result provides a qualitative explanation of the effects induced by low temperature hydrogen fuel injection that decreases gas temperature and provides a certain amount of fresh fuel into the cross stream.

3.6. Jet flame ignition by the pulsed plasma

Figure 10 shows the temperature (Fig. 10a) and radical concentration (Fig. 10b–e) time histories of the H_2/O_2 mixture in the region of interest. As shown in Fig. 10a and b, the temperature and the radical concentrations of the mixture increase in region B in the presence of the plasma while they remain almost unchanged without the plasma, consistent with the experimental observations. It is noteworthy that radical production by the plasma results in only about 10^{-5} in radical mole fractions, while the radical mole fraction in front of the downstream jet (the boundary between the region B and the region C) reaches a level of about 10^{-2}. This confirms that the initial radical seeding by the plasma results in strong increases in the radical pool by the combustion reactions in region B (the pilot flame). In Fig. 10b, we see that the H radical history and the subsequent effect of this pilot flame on the H mole fraction (linear scale), while Fig. 10c–e depict the corresponding mole fractions of H, O, and OH on logarithmic scales, respectively. We see also that the single plasma pulse applied at a time of 7 μs in these frames, causes a sudden increase in the radical (H, O and OH) mole fraction, and is followed by exponential growth in region B. An even greater increase in temperature and the radical concentrations, in this pilot flame region, is seen to be predicted with higher plasma pulse energy (0.4 mJ (20 W, 50 kHz) in comparison to 0.2 mJ (10 W, 50 kHz)).

The difference between the plasma on and off cases becomes more obvious in the predicted properties in region C of the flow. The temperature and the radical mole fraction differences for the two cases (plasma on and off) are once again magnified, in the downstream jet flame region. Rapid increases in temperature and radical mole fractions are predicted in the presence of the plasma while these remain steady (or drop due to recombination) without the plasma, as the flow fails to ignite, as seen in the experiments. The simulations confirm that a low average power plasma discharge (10 W) is capable of igniting the downstream jet flame in this duel fuel jet injection configuration even when it represents a mere fraction (10^{-5}) of the combustion energy release. It is noteworthy that the fuel/oxidizer mixture of approximately 700 K static temperature at the downstream jet injection point is ignited immediately (abrupt temperature rise in the presence of the plasma) aided by the radicals supplied from the pilot flame. The effect of this low power (10–20 W) nonequilibrium plasma-supported pilot flame is comparable to that induced by a thermal plasma of much higher power (over 10 kW), as reported in Ref. [19]. We also note that, the increase in average plasma power (or doubling of the discharge pulse energy) from 10 W to 20 W makes a marked difference in the temperature and the radical production in the leeward side of the downstream jet.

4. Summary and conclusions

The use of low power nonequilibrium nanosecond pulsed discharges to stabilize supersonic combustion has not been widely studied because the typical discharge energy per pulse (~0.2 mJ) is very low in comparison to the flow enthalpy over the time between pulses (~100 J). Instead, previous research [19] incorporates recirculation zones, such as wall cavities, together with these plasma discharges, to enhance ignition and stabilize combustion. Using a dual fuel jet injection configuration, as introduced in this paper, we overcome this limitation by channeling the plasma energy into the activation of a subsonic fuel/oxygen mixture that serves as a pilot flame that subsequently anchors the ignition of the main supersonic flame. This plasma-enhanced supersonic combustion can be interpreted to occur in two stages. The first stage diverts fuel towards an oblique, subsonic injector, which seeds the hot boundary layer with fuel, and the partially mixed boundary layer is then subjected to a low power nanosecond pulsed plasma. Some plasma-enhanced combustion of this stream takes place (as evidenced by OH PLIF). Radical production by this "pilot flame" (order of 10^{-2}–10^{-3} in mole fraction at the end of region B (pilot flame region) as seen in Fig. 10c–e) representing several orders of magnitude more than can be obtained by the discharge alone (order of 10^{-5} at the start of region B as seen in Fig. 10c–e), serves then, in the second stage, to ignite and sustain the combustion of the majority of the fuel, which is introduced downstream of the plasma.

This approach to supersonic combustion is easily integrated into a flat wall, and does not require the introduction of wall features to generate flow recirculation, hence minimizing stagnation pressure losses. In addition, we show that the plasma assisted pilot flame is capable of flame-holding in the windward/leeward side of the main jet over a test time of approximately 300 μs, and appears to maintain combustion even during the time between discharge pulses (20 μs).

Acknowledgments

This work is sponsored by the AFOSR/MURI Program–Experimental/Computational Studies of Combined-Cycle Propulsion: Physics and Transient Phenomena in Inlets and Scramjet Combustors with Julian Tishkoff as the Technical Monitor.

References

[1] A. Ben-Yakar, R.K. Hanson, J. Propul. Power 17 (2001) 869–877.
[2] C.C. Rasmussen, J.F. Driscoll, C.D. Carter, K.Y. Hsu, J. Propul. Power 21 (2005) 765–768.
[3] M.R. Gruber, J.M. Donbar, C.D. Carter, K.Y. Hsu, J. Propul. Power 20 (2004) 769–778.
[4] L. Maddalena, T.L. Campioli, J.A. Schetz, AIAA-2005-3235, in: AIAA/CIRA 13rd Int. Space Planes and Hypersonics Systems and Tech. Conf., Capua, Italy, 2005.
[5] C.D. Anderson, J.A. Schetz, J. Propul. Power 21 (2005) 371–374.
[6] S.B. Leonov, D.A. Yarantsev, A.P. Napartovich, I.V. Kochetov, IEEE Trans. Plasma Sci. 34 (2006) 2514–2525.
[7] R.C. Rogers, D.P. Capriotti, R.W. Guy, AIAA-98-2506, in: 20th AIAA Advanced Measurement and Ground Testing Tech. Conf., Albuquerque, NM, 1998.
[8] C.D. Cathey, T. Tang, T. Shiraishi, T. Urushihara, A. Kuthi, M.A. Gundersen, IEEE Trans. Plasma Sci. 35 (2007) 1664–1668.
[9] S.A. Bozhenkov, S.M. Starikovskaia, A. Yu Starikovskii, Combust. Flame 133 (2003) 133–146.
[10] V.P. Zhukov, A.E. Rakitin, A. Yu Starikovskii, AIAA 2007-1029, in: 45th AIAA Aerospace Sciences Meeting and Exhibit, Reno, NV, 2007.
[11] W. Kim, M.G. Mungal, M.A. Cappelli, Appl. Phys. Lett. 92 (2008) 051503.
[12] W. Kim, H. Do, M.G. Mungal, M.A. Cappelli, AIAA 2006-560, in: 44th AIAA Aerospace Sciences Meeting and Exhibit, Reno, NV, 2006.
[13] W. Kim, H. Do, M.G. Mungal, M.A. Cappelli, IEEE Trans. Plasma Sci. 34 (2006) 2545–2551.
[14] W. Kim, H. Do, M.G. Mungal, M.A. Cappelli, Proc. Combust. Inst. 31 (2007) 3319–3326.
[15] W. Kim, H. Do, M.G. Mungal, M.A. Cappelli, Combust. Flame 153 (2008) 603–615.
[16] A. Bao, Y.G. Utkin, S. Keshav, G. Lou, I.V. Adamovich, IEEE Trans. Plasma Sci. 35 (2007) 1628–1638.
[17] G.L. Pilla, D.A. Lacoste, D. Veynante, C.O. Laux, IEEE Trans. Plasma Sci. 36 (2008) 940–941.
[18] I.I. Esakov, L.P. Grachev, K.V. Khodataev, V.A. Vinogradov, D.M. Van Wie, IEEE Trans. Plasma Sci. 34 (2006) 2497–2506.
[19] H. Do, M.A. Cappelli, M.G. Mungal, Combust. Flame 157 (2010) 1783–1794.
[20] H. Do, M.G. Mungal, M.A. Cappelli, IEEE Trans. Plasma Sci. 36 (2008) 2918–2923.
[21] W.N. Heltsley, J.A. Snyder, A.J. Houle, D.F. Davidson, M.G. Mungal, R.K. Hanson, AIAA 2006-4443, in: 42nd AIAA/ASME/SAE/ASEE Joint Propulsion Conf. and Exhibit, Sacramento, CA, 2006.

[22] H. Do, Ph.D. dissertation, Mechanical Engineering Department, Stanford University, Stanford, CA, 2009.
[23] G.S. Settles, Schlieren & Shadowgraph Techniques, Springer-Verlag, New York, 2006.
[24] W.N. Heltsley, J.A. Snyder, M.G. Mungal, R.K. Hanson, in: 14th Int. Symp. on Application of Laser Techniques to Fluid Mechanics, Lisbon, Portugal, 2008.
[25] <http://www.siglo-kinema.com/bolsig.htm>.
[26] S.J.B. Corrigan, J. Chem. Phys. 43 (1965) 4381–4386.
[27] D.A. Vroom, F.J. de Heer, J. Chem. Phys. 50 (1969) 580–590.
[28] B.M. Penetrante, M.C. Hsiao, B.T. Merritt, G.E. Vogtlin, P.H. Wallman, M. Neiger, O. Wolf, T. Hammer, S. Broer, Appl. Phys. Lett. 68 (1996) 3719–3721.
[29] M.S. Bak, W. Kim, M.A. Cappelli, Appl. Phys. Lett., submitted for publication.
[30] S. Kawai, S. Lele, Center for Turbulence Research Annual Research Briefs (2008) 139–151.